Fermi Surface of Nanocrystalline Embedded Particles in Materials: bcc Cu in Fe

Y. Nagai,[1] T. Chiba,[2] Z. Tang,[3] T. Akahane,[2] T. Kanai,[1] M. Hasegawa,[1,3] M. Takenaka,[4] and E. Kuramoto[4]

[1]*The Oarai Branch, Institute for Materials Research, Tohoku University, Oarai, Ibaraki 311-1313, Japan*
[2]*Advanced Materials Laboratory, National Institute for Materials Science, Tsukuba 305-0044, Japan*
[3]*Institute for Materials Research, Tohoku University, Sendai 980-8577, Japan*
[4]*Research Institute for Applied Mechanics, Kyushu University, Fukuoka 816-8580, Japan*

(Received 19 March 2001; published 5 October 2001)

We report that a positron can act as a probe to directly reveal electronic structures of nanocrystalline embedded particles in materials. The Fermi surface (FS) of "bcc" Cu nanoparticles in an Fe matrix is observed as the first example. A two-dimensional angular correlation of the positron annihilation radiation (2D-ACAR) method is used to measure the momentum distribution which reflects the FS topology. The obtained 2D-ACAR spectra show strong and characteristic anisotropy associated with the necks of the FS around the {110} Brillouin zone boundaries of the bcc Cu, which are well reproduced by full-potential linearized argumented plane-wave calculations.

DOI: 10.1103/PhysRevLett.87.176402 PACS numbers: 71.18.+y, 73.22.–f, 78.70.Bj

The nanocrystalline embedded particle (NCEP) in material is one of the current attractive subjects because of not only their application prospects as quantum devices but also the fundamental interest in mesoscopic systems. In many cases, the atomic structures of the nanocrystals are different from the bulk ones since they are strongly affected by the environmental host materials. It is therefore of great interest to study the electronic structures of such NCEPs. However, there was no experimental tool so far to reveal them directly because the probes employed in conventional methods have no site selectivity; the probes equally interact with both the NCEPs and the host materials, causing difficulty to extract unambiguously the weak interaction signals of the NCEPs from a much stronger background of the host. In order to study the NCEPs, therefore, the probe which seeks them by itself and provides exclusive information on them is very necessary.

Recently, we have found that a positron, an antiparticle of an electron, is the site-selective probe for the NCEPs. It is well known that the positron is sensitive to vacancy-type defects. However, we have confirmed that the positron can be confined in the NCEPs with positron affinities [1,2] higher than that of the host even if the NCEPs are free from such defects [3]. We call this affinity-induced confinement the positron quantum-dot-like state. The positron in the quantum-dot-like state annihilates with an electron of the NCEPs exclusively and provides us site-selective information on their electronic structure with the two emitted gamma photons. The highlight of this Letter is the observation of the Fermi surface (FS) of bcc Cu nanocrystals embedded coherently in bcc Fe using the positron annihilation method as the first example of the electronic structure study of the NCEPs (see Fig. 1).

The two-dimensional angular correlation of positron annihilation radiation (2D-ACAR) is one of the best methods to reveal FS [4,5]. By measuring the 2D angle distribution between the two emitted photons, we can obtain 2D projection of the electron momentum distribution, which reflects the FS topology directly. In particular, the anisotropy of the 2D-ACAR spectrum, which is defined as the differences between an observed 2D-ACAR and its cylindrical average, highlights the feature of the FS shape. Figure 2(a) shows the well-known FS of bulk Cu (fcc structure); the FS bulges out in the $\langle 111 \rangle$ direction and has eight necks at the center of the hexagonal {111} Brillouin zone (BZ) boundaries (L point). The detail of this FS shape has been revealed by the 2D-ACAR measurements. Figure 2(b) shows the anisotropy of the 2D-ACAR corresponding to the (100) plane projection of the momentum distribution. Four peaks just correspond to the necks at the L point. Each peak arises from the overlapped projections of two necks.

While the above result is from the bulk material, we can obtain the FS of metallic NCEP in material by utilizing the positron quantum-dot-like state. Since the positron affinity of the bcc Cu is higher than that of the bcc Fe [2] and we have already found out experimentally that the positron quantum-dot-like state is realized [3] for the bcc Cu in Fe, this system is a good example to demonstrate the ability of the positron annihilation method as a probe for the NCEPs. We show that the FS of the bcc Cu reflecting the BZ shape of the bcc structure has a pronounced different shape from that of the bulk fcc Cu.

The Cu nanocrystals embedded in Fe were obtained by thermal aging a single crystal of a dilute Fe-Cu alloy (Fe-1.0 wt % Cu). The single crystal was prepared from high-purity Fe (4N) and Cu (5N) by arc melting, followed by the strain-annealing method. A single crystal of $\sim$2 mm $\times$ 3 mm $\times$ 0.4 mm in size was then cut off. It was heated to 825 °C and kept 4 h, followed by quenching into ice water. Cu atoms were isolated in a supersaturated solid solution in the as-quenched state. The sample was thermally aged at 550 °C for 0.1 h after quenching; the Cu atoms are aggregated to form nanocrystals (about 1 nm in diameter) coherent to the bcc Fe matrix, suggested by extended x-ray-absorption fine structure [6] and positron

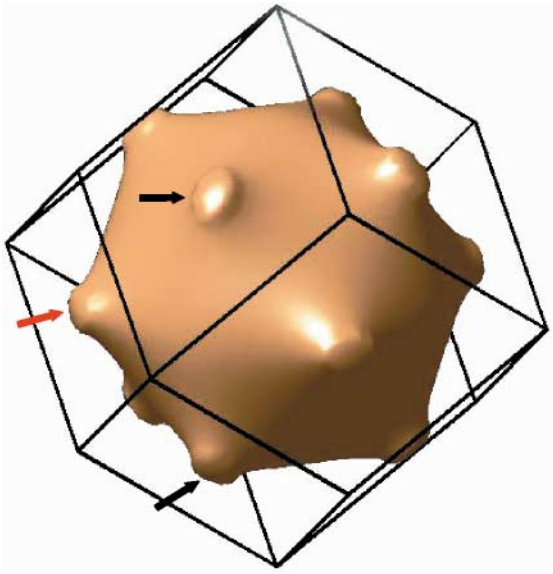

FIG. 1 (color). 3D plot of the FS of bcc Cu calculated by FLAPW (full-potential linearized augmented plane wave) calculations described in the text. The FS has twelve necks at the center of the {110} Brillouin zone boundaries (N point). The neck marked by a red arrow and the two necks marked by black arrows correspond to the peaks in Fig. 4(a) (the anisotropy of the 2D-ACAR spectrum projected along the [100] direction) marked by red and black arrows, respectively.

annihilation experiments [3] using polycrystalline Fe-Cu alloys. The number density of the embedded Cu nanocrystal is estimated to be of the order of 10^{17} cm^{-3} according to our previous work [3]. The aging time of 0.1 h was employed in order that the Cu aggregations certainly form but do not grow so large that they undergo transformations such as bcc to a twinned 9R or fcc structure [7–9].

The 2D-ACAR was obtained using the Anger-camera-type machine [10]. The spectra corresponding to the (100) and (110) plane projections of the momentum distribution were measured although only the data for the (100) plane projection are shown in this Letter. About 5×10^7 counts of the positron annihilations were accumulated for each spectrum. The 2D-ACAR spectra were normalized to the same total counts and smoothed to have the final momentum resolution of about 0.15 a.u. (FWHM); then the anisotropies were obtained.

First, we show the anisotropies of the 2D-ACAR spectra of pure Fe and as-quenched Fe-Cu in Figs. 3(a) and 3(b), respectively, as a reference for the bcc Cu. Since the positron is not trapped at the isolated Cu atoms in the as-quenched state [3], Fig. 3(b) reflects the electronic structure of the "very" dilute Fe-Cu alloy. Thus it is reasonable that both have nearly the same distribution. It is also shown that the anisotropies are much weaker than that for bulk fcc Cu in the momentum area corresponding to the first BZ [Fig. 2(b)].

The anisotropy of the 2D-ACAR for the Fe-Cu aged at 550 °C for 0.1 h, where the bcc Cu nanocrystals form, is

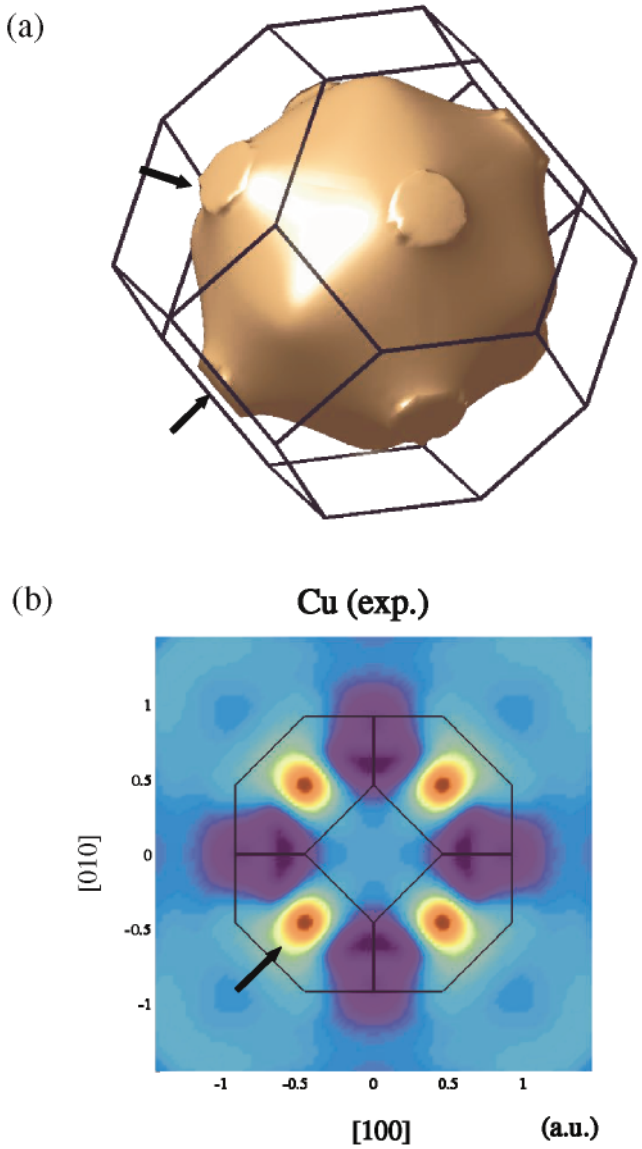

FIG. 2 (color). 3D plots of (a) the FS of bulk Cu (fcc structure) calculated by FLAPW calculations and (b) anisotropy of experimental 2D-ACAR projected along the [100] direction. The four peaks in the plot of the anisotropy correspond to the eight necks at the center of the {111} Brillouin zone boundaries (L point); the marked peak (arrow) in (b) arises from the two necks (arrows) in (a). The color scale is determined so that dark red and dark blue are assigned to the top of the peaks and the bottom of the valleys, respectively.

shown in Fig. 3(c). The characteristic of the anisotropy is different from both anisotropies of bulk Cu [Fig. 2(b)] and bulk Fe [Fig. 3(a)]; this is due to the difference in the electronic momentum distributions between the bcc Cu and Fe. We should consider that the observed 2D-ACAR spectrum consists of the components of both bulk Fe and the bcc Cu nanocrystals. The anisotropy shown in Fig. 3(c) is stronger in the momentum area corresponding to the first BZ (within ~0.8 a.u. from the center), whereas it is weaker outside of this area as compared with that for bulk

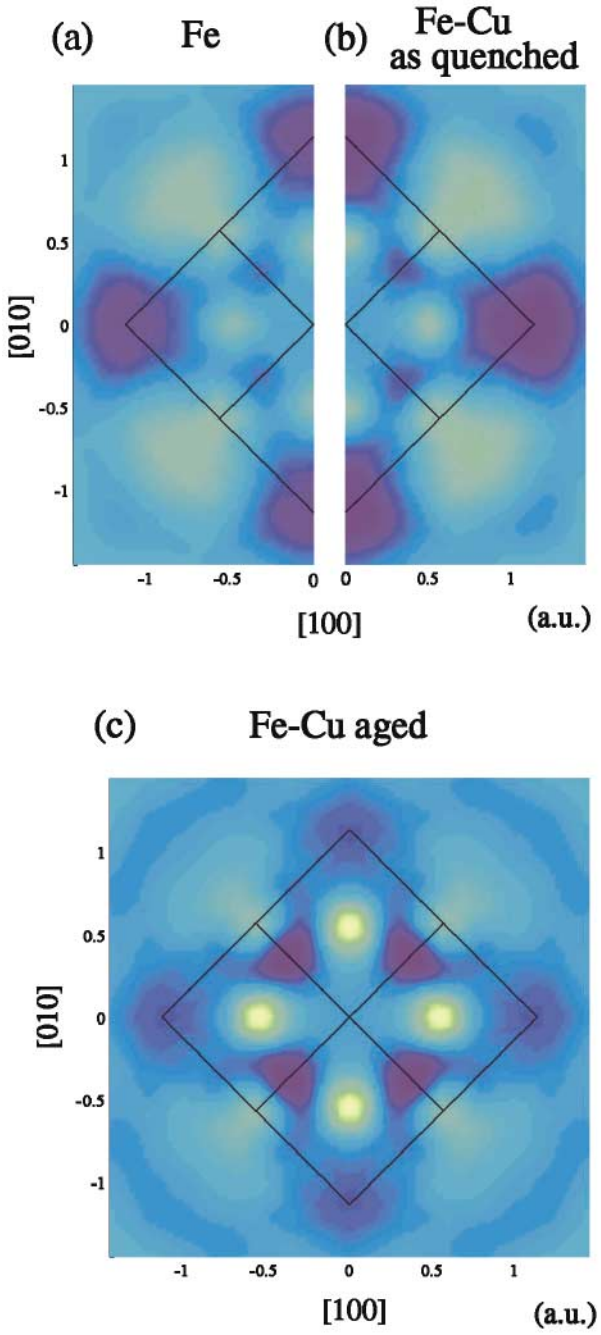

FIG. 3 (color). 3D plots of anisotropies of experimental 2D-ACAR projected along the [100] direction for (a) bulk Fe (bcc structure), (b) Fe-1.0 wt % Cu as quenched, and (c) Fe-1.0 wt % Cu aged at 550 °C for 0.1 h. The color scales are common to that of Fig. 2(b).

Fe shown in Fig. 3(a). The origin of the anisotropy in the outside area is the 3D electrons in host Fe. The Cu 3D electrons are in filled core states and are much less anisotropic. Thus we estimated the contribution from the bulk Fe by least-squares fitting to reproduce the anisotropy for the bulk Fe [Fig. 3(a)] in the momentum area between 0.8 and 2.5 a.u. from the origin. About half of the positrons are estimated to annihilate with the electrons of the bulk Fe in this case. The detail of the decomposition is described in Ref. [10].

Figure 4(a) is the anisotropy of the 2D-ACAR for the bcc Cu extracted from the total 2D-ACAR by subtracting the bulk Fe component. The four strong peaks and four weak peaks at the momenta corresponding to the projection of the center of the {110} BZ boundaries (N point) are clearly observed; each strong peak arises from the overlap of two necks and each weak peak arises from one neck corresponding to the {110} BZ boundary perpendicular to the (100) projection plane.

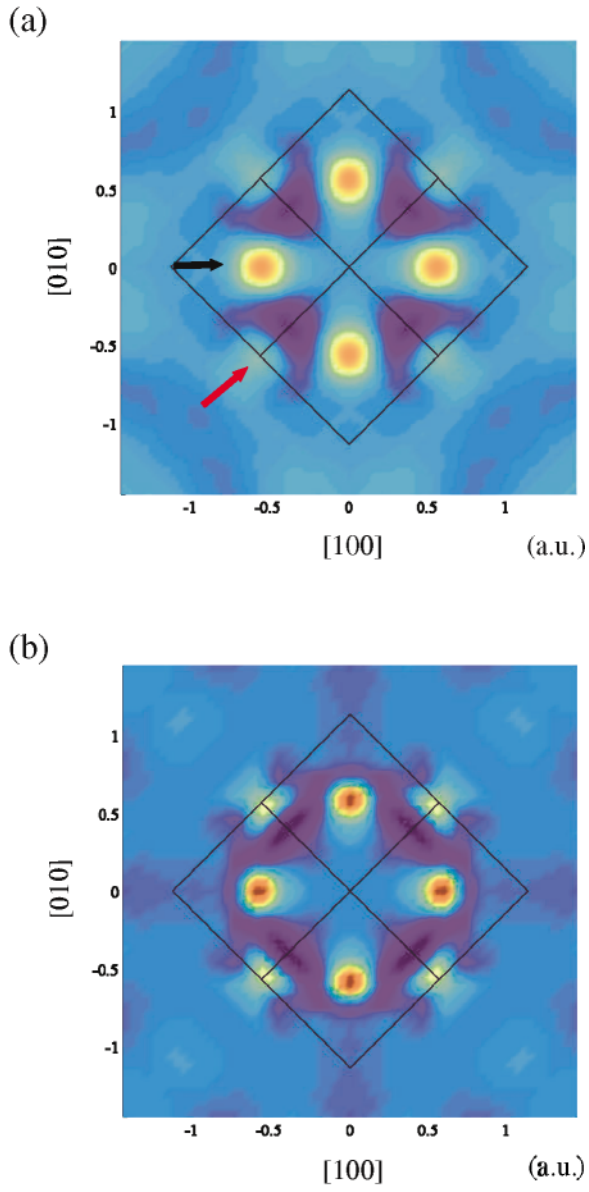

FIG. 4 (color). 3D plots of anisotropies of 2D-ACAR projected along the [100] direction for bcc Cu: (a) experimentally extracted and (b) calculated. The color scales are common to that of Fig. 2(b). The anisotropies have two kinds of peaks: one (black arrow) arises from the two necks marked by black arrows in Fig. 1 and the other (red arrow) arises from the neck marked by a red arrow in Fig. 1.

In order to make sure theoretically of this feature of the FS and visualize the FS, we performed the first-principles calculations of the band structure and the 2D-ACAR for the bcc Cu and fcc Cu, using the FLAPW method [11–13] implemented within the frame of the two-component density functional theory. In our approach, space is divided into atom centered muffin-tin (MT) spheres and remaining interstitial regions. The electron wave functions are expanded by the LAPW basis functions, which are represented as spherical functions inside the MT spheres and plane waves in the interstitial regions. The positron wave function is expanded by plane waves over the whole solids. The sizes of the basis sets are carefully chosen so that the convergence of total energy in all the calculations is better than 0.1 mRy. The electron exchange and correlation (the positron-electron correlation) are (is) treated within the local spin density (the local density) approximation [14–16]. The BZ integrations for the electron charge densities are performed using the special k points scheme [17]. In the calculations, the experimental lattice parameters of fcc Cu (3.61 Å) and the optimized lattice parameter for bcc Cu (2.90 Å) are employed. By projecting the 3D momentum densities along the chosen axes of the experiments, the 2D-ACAR distributions are then obtained. The present method is found to be highly reliable because we have confirmed that the calculated 2D-ACAR for fcc Cu well reproduces the experimental data [Fig. 2(b)]. The calculated anisotropy of the 2D-ACAR of bcc Cu is shown in Fig. 4(b), which well reproduces the experimental data [Fig. 4(a)]. We also found that the 2D-ACAR spectra of (110) projection planes agree well with the corresponding calculations. The FS obtained from the calculated band structure is shown in Fig. 1. The twelve necks at the center of the {110} BZ boundaries (N point) are clearly observed. The necks seem narrower than those in the case of the fcc Cu.

In summary, the FS of the bcc Cu in bcc Fe matrix is directly observed, which shows that the positron annihilation provides us with a unique method to probe the electronic structure of the nanocrystals embedded in materials. It is expected that the finite size effect on the electronic structure would be observed by the measurement at low temperature, which is an attractive future work. The size of the nanocrystals could be controlled by the precise heat treatment in the Fe-Cu system. The affinity-induced positron confinement occurs whenever the positron affinity for the embedded nanocrystals is higher than that for the host materials. Therefore we can apply this method to other systems such as nanoquantum devices.

This work is partially supported by JAERI's Nuclear Research Promotion Program (JANP) and Grant-in-Aid for Scientific Research of the Ministry of Education, Science and Culture (No. 10450229, No. 11750565, No. 12358005, and No. 12640334). We thank Professor Y. Kawazoe and the Information Science Group of the Institute for Materials Research, Tohoku University for their continuous support for using the supercomputing system. We thank Mr. T. Takahashi for preparing the samples by arc melting.

[1] M. J. Puska and R. M. Nieminen, Rev. Mod. Phys. **66**, 841 (1994).
[2] G. Brauer, M. J. Puska, M. Sob, and T. Korhonen, Nucl. Eng. Des. **158**, 149 (1995).
[3] Y. Nagai, M. Hasegawa, Z. Tang, A. Hempel, K. Yubuta, T. Shimamura, Y. Kawazoe, A. Kawai, and F. Kano, Phys. Rev. B **61**, 6574 (2000).
[4] K. Fujiwara and O. Sueoka, J. Phys. Soc. Jpn. **21**, 1947 (1966).
[5] *Positron Spectroscopy of Solids,* edited by A. Dupasquier and A. P. Mills, Jr. (IOS Press, Amsterdam, 1995).
[6] S. Pizzini, K. J. Roberts, W. J. Phythian, C. A. English, and G. N. Greaves, Philos. Mag. Lett. **61**, 223 (1990).
[7] W. J. Phythian and C. A. English, J. Nucl. Mater. **205**, 162 (199), and references therein.
[8] P. J. Othen, M. L. Jenkins, and G. D. W. Smith, Philos. Mag. A **70**, 1 (1994).
[9] G. R. Odette, C. L. Liu, and B. D. Wirth, Mater. Res. Soc. Symp. Proc. **439**, 457 (1997), and references therein.
[10] M. Hasegawa, T. Chiba, A. Kawasuso, T. Akahane, M. Suezawa, S. Yamaguchi, and K. Sumino, Mater. Sci. Forum **199–201**, 1481 (1995).
[11] H. J. F. Jansen and A. J. Freeman, Phys. Rev. B **30**, 561 (1984).
[12] L. F. Mattheiss and D. R. Hamann, Phys. Rev. B **33**, 823 (1986).
[13] P. Blaha and K. Schwarz, J. Phys. F **17**, 899 (1987).
[14] E. Boronski and R. M. Nieminen, Phys. Rev. B **34**, 3820 (1986).
[15] M. J. Puska and R. M. Nieminen, Rev. Mod. Phys. **64**, 841 (1994).
[16] Z. Tang, M. Hasegawa, T. Chiba, M. Saito, A. Kawasuso, Z. Q. Li, R. T. Fu, T. Akahane, Y. Kawazoe, and S. Yamaguchi, Phys. Rev. Lett. **78**, 2236 (1997).
[17] D. J. Chadi and M. L. Cohen, Phys. Rev. B **8**, 5747 (1973).